Published online 2 August 2013 *Nucleic Acids Research, 2013, Vol. 41, No. 19* ***8979–8994***
doi:10.1093/nar/gkt670

XPD-dependent activation of apoptosis in response to triplex-induced DNA damage

Meetu Kaushik Tiwari and Faye A. Rogers*

Department of Therapeutic Radiology, Yale University School of Medicine, New Haven, CT 06520, USA

Received November 28, 2012; Revised May 20, 2013; Accepted May 26, 2013

ABSTRACT

DNA sequences capable of forming triplexes are prevalent in the human genome and have been found to be intrinsically mutagenic. Consequently, a balance between DNA repair and apoptosis is critical to counteract their effect on genomic integrity. Using triplex-forming oligonucleotides to synthetically create altered helical distortions, we have determined that pro-apoptotic pathways are activated by the formation of triplex structures. Moreover, the TFIIH factor, XPD, occupies a central role in triggering apoptosis in response to triplex-induced DNA strand breaks. Here, we show that triplexes are capable of inducing XPD-independent double strand breaks, which result in the formation of γH2AX foci. XPD was subsequently recruited to the triplex-induced double strand breaks and co-localized with γH2AX at the damage site. Furthermore, phosphorylation of H2AX tyrosine 142 was found to stimulate the signaling pathway of XPD-dependent apoptosis. We suggest that this mechanism may play an active role in minimizing genomic instability induced by naturally occurring noncanonical structures, perhaps protecting against cancer initiation.

INTRODUCTION

An intricate balance between DNA repair and apoptosis has evolved to protect the integrity of the human genome against the potentially devastating effects of endogenous and exogenous genotoxins. Decisions to activate either pathway in response to DNA damage minimize the likelihood of genomic instability, which can lead to mutagenesis and ultimately to carcinogenesis. Although the regulatory mechanisms and signaling pathways controlling DNA repair and apoptosis are well characterized, the driving forces responsible for making the ultimate choice between DNA repair and cell survival or apoptotic cell death in response to genotoxic stress remain unclear. Key proteins that contribute to cellular survival by acting in DNA repair can become executioners in the face of excess DNA damage. Studies suggest that some proteins required for efficient nucleotide excision repair (NER) may also play a role in apoptosis (1). The XPD protein has been identified as having two primary functions in NER: (i) stabilization of the transcription factor complex TFIIH and (ii) 5′→ 3′ helicase function (2). In addition to its function in NER, transcription and possibly cell cycle regulation, XPD is also required for p53-mediated apoptosis (3–5).

The NER pathway occupies an important position in the recognition and repair of a wide array of helix-distorting lesions. Previous studies have shown that high-affinity DNA-binding molecules can create helical distortions upon binding to duplex DNA that strongly provoke NER-dependent repair (6,7). However, it was unknown whether formation of these structures caused a severe enough alteration in the DNA double helix to trigger activation of apoptotic pathways. Triplex DNA is formed when triplex-forming oligonucleotides (TFOs) bind as third strands in a sequence-specific manner within the major groove of duplex DNA at polypurine stretches. These molecules provide a means to experimentally create bulky helical distortions that are subject to NER and afford an opportunity to evaluate cellular responses to increasing levels of structurally induced DNA damage.

The human genome includes DNA sequence patterns that can adopt a variety of alternative structures in addition to the B-conformation described by Watson and Crick (8). For example, H-DNA (triplex) formation is favored by sequences that contain mirror repeat symmetry and occurs at purine/pyrimidine tracts (9–11). Naturally occurring sequences capable of forming H-DNA are found in the human genome as frequently as 1 in every 50 000 base pairs (12). Formation of these structures cause severe genomic alterations and represent an endogenous source of genotoxic stress (12,13). For instance, the H-DNA forming sequence located in the promoter region of the *c-myc* gene has been implicated

*To whom correspondence should be addressed. Tel: +1 203 737 3658; Fax: +1 203 737 6309; Email: faye.rogers@yale.edu

in the translocation of the gene in Burkitt's lymphoma (14). Because the triplex region found in endogenous H-DNA is similar in structure to intermolecular triplexes formed by TFOs, they represent an excellent model to study the molecular pathways that determine cellular fate in response to endogenous sources of genotoxic stress.

In the present work, we have determined that the formation of triplex structures can indeed provoke apoptotic responses and reveal an XPD-dependent mechanism that modulates survival/apoptotic decisions in response to structurally induced DNA damage. In conjunction with the use of an established cell line and a transgenic mouse model containing multiple chromosomal target sites, sequence-specific TFOs were used to synthetically create altered helical structures. Our studies demonstrate that triplex-induced double strand breaks (DSBs) can stimulate cells to activate apoptosis both *in vitro* and *in vivo*. Although knockdown of XPD did not modulate the extent of triplex-induced DSBs, its depletion resulted in a decrease in triplex-induced apoptosis. Further investigation determined that XPD is recruited to the H2AX serine 139 phosphorylation site and its presence is required for the phosphorylation of the H2AX tyrosine 142 residue, which has been shown to be an essential post-translational modification for the recruitment of pro-apoptotic factors to the tail of γH2AX. These results identify a new role for XPD in addition to its previously reported requirement for p53-mediated apoptosis in regulating cellular fate decisions. Our findings suggest that XPD-dependent apoptosis plays a key role in preserving genomic integrity in the presence of excessive structurally induced DNA damage.

MATERIALS AND METHODS

Oligonucleotides

Oligonucleotides were synthesized with a 3′-amino-modifier C7 CPG (Glen Research) by the Midland Certified Reagent Company Inc. and purified by RP-HPLC. The sequence of the TFO, AG30, used in our studies along with its target site are depicted in Figure 1A. The G-rich TFO was also synthesized with the guanines in A8$\mathcal{G}$30 replaced with 7-deaza-8-aza-guanine (PPG, $\mathcal{G}$, Glen Research) as indicated in Figure 1F. Third strand binding of the TFO to duplex DNA was measured by gel mobility assays as previously described (15). The control oligonucleotide, MIX30, a mixed base 30-mer, has the following sequence: 5′-AGT CAGTCAGTCAGTCAGTCAGTCAGTCAG-3′.
Labeled oligonucleotides were synthesized with 5′-rhodamine modifications using rhodamine phosphoramidite.

Cells lines and transfections

C127 cells were obtained from ATCC. The mouse epithelial cell line, AV16, containing ~100 randomly integrated chromosomal copies of the triplex target site was derived from the parental C127 cell line, and target site copy number was determined using quantitative DNA dot blot analysis as previously described (16). A mouse fibroblast cell line with the λsupFG1 vector chromosomally integrated and deficient in XPA was derived from transgenic mice carrying the λsupFG1 vector as a transgene and targeted disruptions in the NER gene, XPA. A similar cell line containing the λsupFG1 vector was derived from wild-type mice and used for comparison.

Cells were seeded in six-well plates at a density of 2×10^5 cells per well the day before transfection. Cells were transfected with 2 μg of AG3O or MIX30 using Oligofectamine (Invitrogen) transfection reagent. Transfection was performed as per manufacturer's instructions. siRNA directed against XPD, GAPDH and nontarget controls (ON-Target plus SMARTpool reagents; Dharmacon) were transfected into AV16 cells using Dharmafect-1 transfection reagent (Dharmacon) according to the manufacturer's instructions. Western blot analysis was used to confirm knockdown of protein.

AV16 cells were used to generate XPD−/− cells using shRNA. Briefly, lentivirus shRNA vectors for XPD knockdown were obtained from Sigma-Aldrich (XPD-18: TRCN0000071118; XPD-19: TRCN0000071119; XPD-58: TRCN0000338058). AV16 cells were transduced with Lentiviral expression constructs either for nontarget shRNA or GFP shRNA or one of the three different shRNA targeting XPD (ERCC2). Stable clones expressing the shRNA were established via puromycin dihydrochloride selection (2 μg/ml). AV16 clone XPD-19-1 stably expressing shRNA XPD-19 was used in the mutagenesis experiments.

Metaphase chromosome spreads

AV16 cells were transfected with 2 μg of rhodamine-labeled MIX30 or AG30. Twenty-four hours posttransfection, cells were treated for 5 h with Colcemid (0.1 μg/μl). Cells were then collected and washed once with PBS. To the cell pellet, a 75 mM KCl solution was added for 20 min at 37°C. Cell pellets were then resuspended in Carnoy's fixative solution (75% methanol, 25% acetic acid). After 10 min incubation at room temperature, the cells were pelleted and resuspended in an additional 500 μl of Carnoy's fixative solution. Cells were dropped from a height onto glass slides and mounting medium with DAPI (Prolong Gold antifade reagent, Invitrogen) was added to each slide. Pictures were taken of 50–60 metaphase spreads using an Axiovert 200 microscope (Carl Zeiss Micro Imaging, Inc.).

Survival assays

Cell survival was assayed either by visualization of monolayer growth or by colony formation. To quantify survival by monolayer growth, cells were seeded at a defined density in either 6 or 12 well dishes and treated with the TFO as previously described. Cells were stained with crystal violet 24, 48 and 72 h posttreatment for monolayer visualization. To assay for cell survival by clonogenic survival, cells were treated with 2 μg of AG3O or MIX30 for 48 h and then seeded at 250–500 cells per well. Colonies were washed with 0.9% saline solution and stained with crystal violet 10–14 days later. Colonies consisting of >50 cells were counted. Colony formation was normalized to plating efficiency of the nontreated

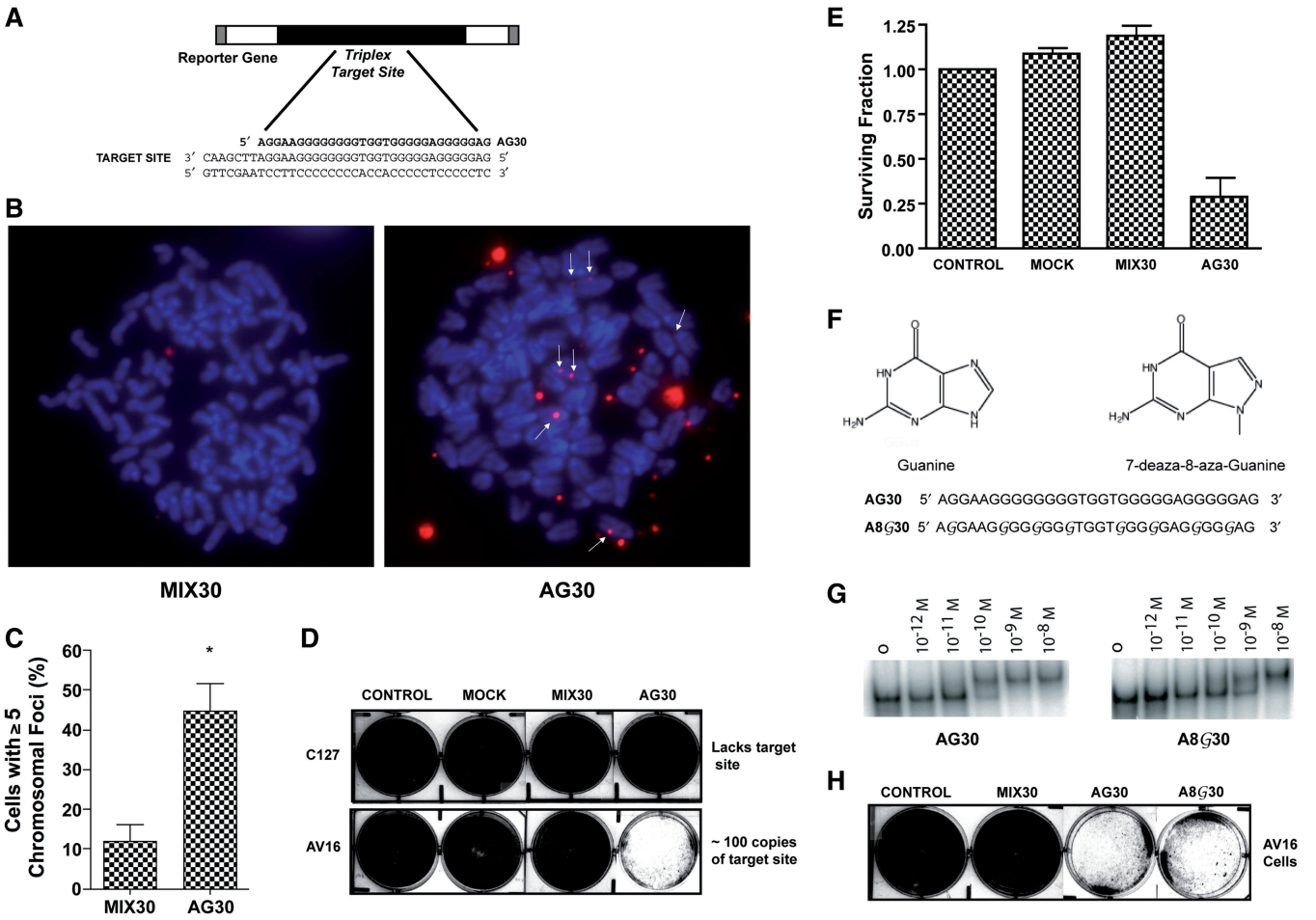

Figure 1. Analysis of triplex-induced cell death. (**A**) Schematic for the generation of synthetic triplex DNA structures. Triplex structures were created using a 30mer TFO, AG30, which has been shown to bind sequence-specifically to the polypurine target sequence. (**B**) Images of a nondenatured metaphase chromosome spread generated from AV16 cells treated with either 2 μg of rhodamine-labeled AG30 or the control oligonucleotide, MIX30. (**C**) Quantification of AG30-induced chromosomal foci. Fifty to sixty metaphase chromosome spreads were analyzed per treatment. $^{*}P < 0.05$. (**D**) The established mouse cell line (AV16) was engineered to contain randomly integrated chromosomal triplex target sites. Cells were treated with 2 μg of TFO and stained with crystal violet 48 h posttreatment. Monolayer growth assays demonstrate a decrease in cell survival that is proportional to an increase in triplex formation. (**E**) Survival by colony formation of AV16 cells following TFO treatment (mean ± SEM, $n = 3$). (**F**) Structure of the natural guanine base compared with the modified base 7-deaza-8aza-guanine (PPG). Sequence of the PPG-substituted 30-mer TFO, A8$\mathcal{G}$30, compared with AG30. $\mathcal{G}$ represents PPG. (**G**) Gel mobility shift assay of triplex formation. The target duplex was end-labeled and incubated with increasing concentrations of the indicated TFO followed by native polyacrylamide gel electrophoresis. (**H**) Monolayer growth assay reveal similar reduction in cell growth following treatment with either 2 μg of AG30 or A8$\mathcal{G}$30.

cells. Errors bars in the survival analysis are based on three independent experiments.

Apoptosis analysis

Cells were analyzed by flow cytometry 24 h posttreatment using the Annexin V-FITC/PI apoptosis detection kit (BD Pharmingen) according to the manufacturer's protocol. The apoptotic rate was calculated as the combined percentage of early apoptotic and late apoptotic cells. Data analysis was performed using FlowJo software.

Western analysis

Floating and adherent cells were collected; cell pellets were lysed with RIPA buffer (150 mM NaCl, 0.1% SDS and inhibitors); and 30–50 μg of total protein per sample was resolved by SDS-PAGE. Proteins were detected by a standard immunoblot protocol using the following primary antibodies: cleaved PARP; cleaved caspase 3; phospho-p53 (serine 15); phospho-H2AX (serine 139) (Cell Signaling Technology, Inc. Danvers, MA); phospho-H2AX (tyrosine 142) (Millipore Corporation, Billerica, MA); XPD (BD Biosciences, San Jose, CA); tubulin (clone B-512; Sigma, St. Louis, MO). Each experiment was carried out a minimum of three times, and representative Western blots are shown.

Immunofluorescence

Cells, seeded onto UV-irradiated coverslips, were treated for 24 h, and samples were prepared under reduced light as previously described (17). Cells were incubated with the following antibodies: rabbit anti-γH2AX antibody (Cell Signaling) and FITC-conjugated F(ab′)2 fragment

donkey anti-rabbit IgG (H + L) (Molecular Probes Inc.), and then stained with 100 ng/ml DAPI (Sigma). Images were captured using an Axiovert 200 microscope (Carl Zeiss Micro Imaging, Inc.).

Neutral comet assay

Cells were collected 24 h posttreatment, and neutral comet assays were performed according to the manufacturer's protocol (Trevigen Inc), with one adjustment of 3.5×10^5 cells/ml for each single cell suspension. Comets were visualized using an Axiovert 200 microscope and analyzed with Comet Score^{TM} software (TriTek Corp). Approximately 100–150 randomly selected nonoverlapping cells were analyzed per experiment. Results were expressed as mean tail moment.

In vivo analysis of triplex-induced DNA strand breaks

AV mice were derived from the CD1 background (Charles River Laboratories, Wilmington, MA) and were generated as previously described (18). DNA dot blot analysis confirmed the AV founder mouse to carry ~50 copies of the triplex target site in its genome. AV mice or CD1 control mice (14 days old) were treated by intraperitoneal (i.p.) injection with PBS, MIX30 or AG30 (50 mg/kg). Three mice were used per treatment group. Mice were sacrificed 6 h after treatment, and tissue samples were collected. Spleen tissue was collected and fixed in 4% paraformaldehyde overnight at 4°C, embedded in paraffin and cut into sections for evaluation by immunohistochemistry. Cut sections were stained for phospho-H2AX (Cell Signaling) and activated caspase 3 (Abcam) and analyzed by microscopy. All sections were analyzed and quantified by counting 12 randomly selected sections of the same sample. The number of cells positive for activated caspase 3 and γH2AX were manually counted on digital images of the specimens. The differences in the percentage of positive cells were analyzed by one-way ANOVA and Tukey test as posthoc. Representative depiction of immunohistochemistry is shown. Animal studies were approved and performed according to the guidelines of the Institutional Animal Care and Use Committee of Yale University.

Coimmunoprecipitation

AV16 cells were transfected with AG30 or MIX30, and 24 h posttransfection, cells were lysed in IP lysis buffer (Thermo Scientific). To observe the interaction of XPD with γH2AX, cell lysates were immunoprecipitated with polyclonal rabbit antibody γH2AX (Santa Cruz) or rabbit IgG (Jackson Immunoresearch Lab) using protein A/G beads (Santa Cruz) at 4°C for 90 min. The immunoprecipitated complex was analyzed by immunoblotting.

Cell cycle analysis and γH2AX

AV16 cells were collected at 6 and 24 h following transfection with either MIX30 or AG30. After washing once with PBS, the cells were fixed in 1% paraformaldehyde for 15 min on ice. Cells were centrifuged and fixed in 70% ethanol at −20°C for 2 h. The cells were then washed with BSA-T-PBS (1% w/v Bovine Serum Albumin and 0.2% v/v Triton X-100 in PBS) and incubated with γH2AX antibody (Cell Signaling) in BSA-T-PBS overnight at 4°C. After washing, the cells were incubated with anti-rabbit IgG Fab2 Alexa 488 (Molecular Probes) at room temperature for 1 h in the dark. Cells were washed and the pellet resuspended and incubated at room temperature in PI staining solution (PI/RNase solution, BD) for 15 min. Cells were analyzed by flow cytometry.

Mutagenesis assay

The mouse cell lines were established with multiple chromosomally integrated copies of the recoverable λ supFG1 shuttle vector carrying the *supFG1* reporter gene. Following 48–72 h of TFO treatment, genomic DNA was isolated and incubated with λ *in vitro* packaging extracts for shuttle vector rescue and reporter gene analysis as previously described (16,19). Briefly, functional *supFG1* genes suppress the nonsense mutations in the host bacteria β-galactosidase gene yielding blue plaques in the presence of IPTG and X-Gal. If, however, a mutation occurs in the *supFG1* gene, the amber mutation will not be suppressed and the resulting plaque will be white. Mutation frequency was calculated by dividing the number of colorless mutant plaques by the total number of plaques counted. Experiments were done in triplicate, and standard errors were calculated for the mutation frequencies as indicated by the error bars.

Statistical analysis

Differences in the mean number of γH2AX foci/cell, the number of apoptotic cells and tail moment were analyzed by one-way ANOVA and Tukey test as posthoc. All statistical analyses were performed using Graphpad Prism software. $***P < 0.001$, $**P < 0.01$, $*P < 0.05$.

RESULTS

Triplex-induced cell death

Using an assay to measure the induction of repair synthesis, research has determined that TFOs create a helical distortion upon binding to duplex DNA that strongly provokes DNA repair (6,7). Additional studies have confirmed the importance of the NER pathway in the recognition and repair of TFO-induced DNA alterations (7,20). To investigate the potential for helical distortions to induce apoptosis in cells, we generated a mouse epithelial cell line (AV16) with ~100 copies of randomly integrated chromosomal triplex target sites (Figure 1A) (16). Triplex structures were synthetically generated using the TFO, AG30, which is designed to specifically bind to the polypurine target site (Figure 1A). Through the use of a restriction protection assay, AG30-induced triplex formation has been previously detected at a chromosomally integrated target site (21). To confirm chromosomal binding of AG30 in our cell line, we prepared nondenatured metaphase chromosome spreads from AV16 cells that had been treated. Johnson *et al.* have previously described a method for detecting third-stand

binding to nondenatured fixed metaphase spreads (22). To detect triplex formation *in vivo*, we modified their technique by treating the cells prior to generation of the metaphase chromosome spreads. AV16 cells were treated with either 2 μg of rhodamine-labeled AG30 or the control mixed sequence oligonucleotide MIX30, which cannot bind as a third strand to the target polypurine/polypyrimidine sites in the AV16 cells. Twenty-four hours posttreatment, cells were treated for 5 h with Colcemid and then collected and prepared as nondenatured fixed metaphase chromosome spreads according to the protocol previously described (22). To minimize background fluorescence created by the presence of unbound oligonucleotides and nonspecific binding events, multiple washes were incorporated during the preparation of the metaphase spreads. It has been previously established that the DNA of nondenatured fixed metaphase spreads remains in a duplex state (22). Thus, the generation of chromosomal AG30-foci under the conditions of this assay represents third strand binding to fixed chromosomes with intact DNA double helix. As shown in Figure 1B, several rhodamine-AG30 chromosomal foci were detected 24 h posttransfection in the AV16 cell-derived metaphase spreads, in contrast to the rhodamine-MIX30 treated cells. These results provide evidence for third strand binding by AG30 to multiple chromosomal sites, with 45% of AV16 cells treated with rhodamine-AG30 being positive for $\geq$5 chromosomal foci per cell (Figure 1C) compared with ~10% of cells treated with MIX30. The binding of non-triplex–forming oligonucleotides like MIX30 to DNA requires single stranded targets, as a result one would not expect to see high levels of nonspecific chromosomal interactions with the MIX30 control. This is consistent with the fact that this mixed sequence oligonucleotide cannot form Hoogsteen or reverse Hoogsteen triplexes even at high concentrations *in vitro*. Although, there may be some nonspecific retention of MIX30 leading to low levels of foci formation, this is just background in the assay. Treatment of the parental cell line (C127), which lacks the polypurine/polypyrimidine target site, with rhodamine-AG30 further confirms the specificity of third strand binding (Supplementary Figure S1). Analysis of C127 cell-derived metaphase spreads revealed that ~13% of cells were positive for $\geq$5 chromosomal foci per cell following treatment with either MIX30 or AG30. These results are supportive of our conclusions because both MIX30 and AG30 treatment of C127 cells resulted in the same nonspecific background levels. The specific foci formation by AG30 in this assay provides evidence for third strand binding and triplex formation in the treated AV16 cells. The generation of rhodamine-AG30 foci likely represents several third strand binding events in proximity, and so these results support the formation of multiple triplex structures following AG30 treatment of AV16 cells. To this end, the results from these studies provide evidence that AG30-foci formation represents sequence-specific binding to its polypurine target site.

Following this validation, we proceeded to examine whether triplex formation was capable of inducing death in cells with multiple TFO target sites. The parental cell line, C127, which lacks the target site, served as a control to assess the possibility of nonspecific oligonucleotide interactions that could result in cell death. Forty-eight hours after treatment, monolayer growth assays demonstrated a decrease in cell growth that correlated with the formation of triplex structures, suggesting that DNA helical distortions can lead to cell death (Figure 1D). It is important to note that a decrease in cell growth following TFO treatment was only observed in AV16 cells, which have the potential to acquire multiple triplex structures and not in C127 cells, which lack the triplex-binding site. In addition, growth inhibition was not observed in cells that were treated with the control oligonucleotide, MIX30. To further attribute a decrease in cell survival resulting from triplex formation, clonogenic survival studies were performed using AV16 cells. As expected, we found that only cells treated with AG30 experienced a decrease in cell survival (Figure 1E). As observed in the monolayer assay, nonspecific toxicity was not detected with either the transfection agent (mock treatment) or MIX30. The results obtained from the survival assays establish that helical distortions induced by the formation of triplex structures are capable of inducing cell death.

To investigate the possibility that the observed cell death could be attributed to G-quadruplex formation (23–25), A8$\mathcal{G}$30 was designed with the same sequence as AG30 but with every third guanine substituted with the modified guanine base, 7-deaza-8-aza-guanine (PPG or $\mathcal{G}$) (Figure 1F). Studies have determined that substitution of every third guanine with PPG was sufficient to reduce self-association of TFOs containing long runs of guanines (26). To determine the relative binding affinities of the G-rich TFOs for the target duplex, a gel mobility shift assay was performed (Figure 1G). The K_d for each TFO was estimated as the concentration of TFO at which binding was one-half maximal. As shown in Figure 1G, using buffer conditions that promote triplex formation, both TFOs bound to the target site with high affinity ($K_d \sim 1 \times 10^{-9}$ M). Treatment of AV16 cells with either AG30 or the PPG-substituted TFO, A8$\mathcal{G}$30, resulted in a reduction in cell growth as observed by monolayer growth assay (Figure 1H). Taken together, the inability of the control oligonucleotide to induce cell death and the induction of cell death after treatment with A8$\mathcal{G}$30, show that the increase in cell death observed in the survival assays is a result of a specific and site-directed effect of AG30 binding to the chromosomal target site.

Triplex-induced apoptosis

Studies were then initiated to determine whether the increase in cell death observed in the survival assays following TFO treatment resulted from the activation of a pro-apoptotic pathway. AV16 cells were treated with a mock transfection, MIX30, or AG30 and analyzed for induction of apoptosis 24 h posttreatment by detection of Annexin V binding using flow cytometry. Annexin V binding to exposed phosphatidylserine residues in the cell membrane is an early marker of apoptosis, and 23% of the

AG30-treated cells were determined to be Annexin V positive as a result of triplex-induced helical distortions (Figure 2A). Western blot analysis of caspase-mediated cleavage of Poly(ADP-ribose) polymerase (PARP) was also used to confirm triplex-induced apoptosis. PARP, a nuclear DNA-binding protein that recognizes DNA strand breaks, is a substrate for caspase 3, and its cleavage is an early event in apoptotic response (27). Caspase-mediated cleavage of PARP was only detected in cell lysates isolated from AG30-treated AV16 cells (Figure 2B). To confirm that the observed apoptosis resulted from triplex formation and not generation of G-quadruplexes, production of cleaved PARP was analyzed by Western blot analysis 24 h after transfection with either AG30 or A8*G*30. Similar levels of cleaved PARP were detected in cell lysates isolated from A8*G*30-treated AV16 cells compared with AG30 treatment, suggesting that the observed apoptosis can be primarily attributed to triplex formation (Figure 2C). Triplex-induced apoptosis was detected as early as 6 h and up to 72 h post TFO treatment as determined by Western blot analysis (Figure 2D).

To test the impact of multiple triplex structure formation on the level of induced apoptosis, AV16 cells were exposed to increasing concentrations of AG30. As shown in Figure 2E, the percentage of Annexin V positive cells increased with higher concentrations of TFO treatment. Treatment with a low concentration of AG30 (50 nM) resulted in an Annexin V-positive population of ~ 8%, which was slightly higher than that of background (~ 6%). The percentage of Annexin V-positive cells plateaued at ~ 60% following treatment with 200 nM of AG30. Moreover, no increase in the level of apoptotic cells was observed in the cells treated with increasing concentrations of the control oligonucleotide, further confirming that the observed apoptosis can be attributed to the formation of altered helical structures and not due to nonspecific toxicity generated by the oligonucleotide itself. As shown in Figure 2F, clonogenic survival studies correlate with these results, with the surviving cell fraction decreasing with increasing AG30 concentration. Collectively, these results support a mechanism that alterations to the DNA duplex structure created by the formation of multiple triplex structures is capable of inducing apoptosis.

Triplex-induced DSBs

To determine whether TFO-induced altered helical structures can act as a fragile site resulting in DSBs, we performed neutral comet assays. Single cell 'comets' were observed microscopically after separation of DNA fragments from the cells by electrophoresis (Figure 3A). Using

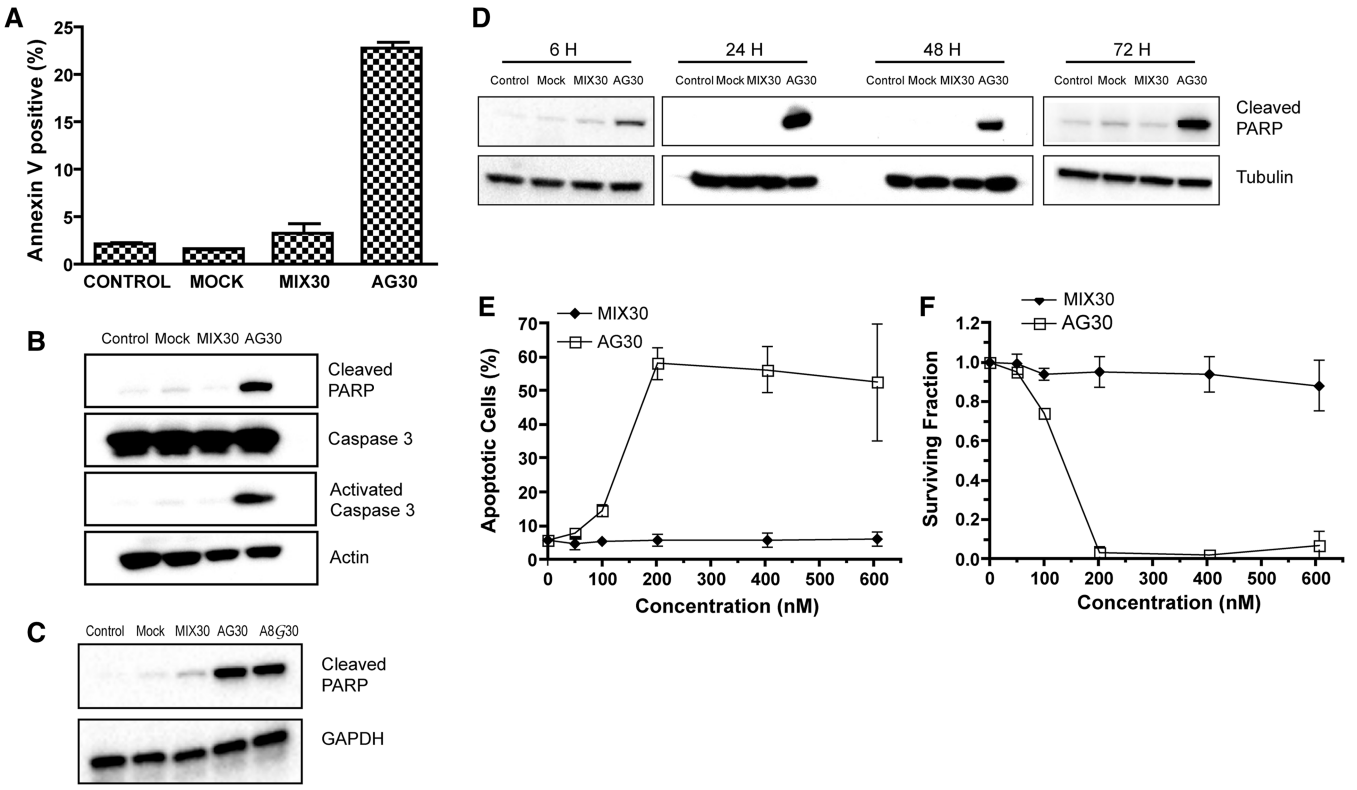

Figure 2. Induction of apoptosis via formation of triplex structures in AV16 cells. (**A**) Annexin V binding to exposed phosphatidylserine residues 24 h after treatment with 2 µg of oligonucleotides. (**B**) Western blot analysis of caspase-mediated cleavage of PARP. Cells were collected and lysates prepared 24 h posttreatment. (**C**) Activation of apoptosis can be attributed to triplex formation rather than G-quadruplex formation as determined by Western blot analysis of cleaved PARP following 2 µg treatment with AG30 or A8*G*30. (**D**) Time course of induced apoptosis by Western blot analysis of cleaved PARP. (**E**) Dose response of increasing concentrations of AG30 and its effect on apoptotic cell death 48 h posttreatment. (**F**) Clonogenic survival after 48 h exposure of AV16 cells to AG30 or MIX30.

the 'comet tail moment' as a measure of the extent of DNA breakage, we assessed the presence of DSBs resulting from triplex formation. As shown in Figure 3A, we determined that AG30 treatment resulted in more DSBs compared with untreated and MIX30-treated cells.

Histone variant H2AX becomes phosphorylated on serine 139 (γH2AX) in response to DNA damage that involves formation of DSBs (28), and foci formation is frequently used as a quantitative marker for DSBs in immunofluorescence microscopy (29). The presence of triplex-induced DSBs was also determined by co-staining for γH2AX and DAPI 24 h after treatment (Figure 3B). AV16 cells treated with AG30 resulted in the formation of more γH2AX nuclear foci compared with untreated cells (Figure 3C). Western blot analysis of γH2AX also confirms the presence of H2AX S139 phosphorylation in only the AG30-treated cells, in agreement with the immunofluorescence results (Figure 3D). These data suggest that the formation of triplex structures in cells that contain multiple target sites generates substantial DSBs, which may overwhelm the cell's repair capacity causing the initiation of an apoptotic response.

To ensure that the presence of γH2AX foci was truly a hallmark of DSBs and not generated in the course of DNA fragmentation during apoptosis, we used a multiparameter cytometry assay (30–32). The presence of triplex-induced DSBs was determined using flow cytometry by staining for γH2AX in the presence of propidium iodine. γH2AX expression attributed to DSBs is cell cycle independent, while high intense γH2AX expression in S-phase is associated with apoptosis (30). Cells were harvested 6 h and 24 h after treatment with AG30. Flow cytometry analysis of γH2AX expression during the cell cycle indicated increased levels of γH2AX in all phases of the cell cycle of AV16 cells 6 h after exposure to AG30 (Figure 3E). This signal persisted for up to 24 h after TFO treatment and increased to 21.7% (Figure 3E), suggesting that many sites marked by γH2AX foci remained unrepaired. Analysis of the flow cytometry profiles indicates that γH2AX expression in AG30-treated cells was significantly higher compared with mock-treated and MIX30-treated cells (Figure 3F).

In Vivo generation of triplex-induced DSBs

To evaluate the potential for triplex DNA to induce DSBs *in vivo*, we used a transgenic mouse model (AV mouse), with ~50 copies of the triplex target sequence chromosomally integrated into its genome (Figure 4A) (18). Immunohistochemistry staining for γH2AX and the apoptosis marker, activated caspase 3, was used to assess the cellular response to *in vivo* triplex formation. AV mice were administered a 50 mg/kg dose of MIX30 or AG30 via i.p. injection. To investigate the extent of triplex-induced DNA strand breaks, we performed immunohistochemistry staining of γH2AX as a marker for ongoing DNA damage on spleen tissue harvested 6 h posttreatment. We observed low levels of γH2AX staining in the spleens of mice that had received i.p. doses of the control oligonucleotide, MIX30 (Figure 4B and C). In contrast, we found that AG30 treatment triggered an increase in the percentage of cells positive for γH2AX foci compared with the PBS- and MIX30-treated mice (Figure 4B and C). To further substantiate the specificity of triplex-induced γH2AX foci, CD1 control mice, which lack the triplex target site, were also administered a 50 mg/kg dose of AG30. Immunohistochemistry analysis of spleen tissue revealed no increase in the percentage of cells positive of γH2AX foci above background (Supplementary Figure S2). An increase in the production of γH2AX foci solely in the AV mice after AG30 treatment would suggest the presence of triplex-induced DSBs. Immunohistochemistry staining for activated caspase 3 was then used to determine whether the formation of triplex-induced γH2AX foci could elicit an apoptotic response *in vivo*. Mice treated with the control oligonucleotide, MIX30, showed almost a complete absence of activated caspase 3 staining in their spleens 6 h following treatment (Figure 4B and D). However, analysis of spleens from AV mice dosed with AG30 revealed that 26% of their spleen cells were positive for activated caspase 3 staining (Figure 4B and D). Examination of spleen tissue samples obtained from CD1 mice treated with AG30 determined a nonexistence of activated caspase 3 6 h posttreatment (Supplementary Figure S2). Altogether, these results are consistent with the interpretation that the formation of endogenous triplex structures can result in DSBs, which can in turn prompt the activation of apoptosis.

NER deficiency results in increased apoptosis levels

Activation of apoptosis in response to DNA damage provides a default mechanism that can be implemented to prevent clonal expansion of cells with unrepaired damage. As a result, studies were initiated to investigate cellular response to triplex-induced DSBs under circumstances where cells may be ineffective at repair. XPA is a key NER factor responsible for verifying altered DNA conformations, and is crucial for correct assembly of the remaining repair machinery around a lesion (33). Previous studies have determined that TFOs were capable of binding to duplex DNA and creating altered helical structures that strongly provoked XPA-dependent DNA repair. To investigate whether triplex formation induced DSBs in an XPA-dependent manner, we treated XPA-proficient and XPA-deficient mouse fibroblast cells with a mock transfection, MIX30 or AG30. Cells were harvested 24 h following treatment, and through the use of flow cytometry, we evaluated the levels of triplex-induced DNA strand breaks by staining for γH2AX. Analysis of γH2AX expression levels as a measure of double strand break formation indicated increased levels of γH2AX in both the XPA-proficient and -deficient cells following AG30 treatment (Figure 5A). Exposure to AG30 increased γH2AX expression in XPA-proficient cells to 22%, and a similar expression level of 28% was observed in the XPA-deficient cells (Figure 5A).

We then proceeded to evaluate induced apoptosis levels as a result of triplex-induced DNA strand breaks in XPA-deficient cells. XPA-deficient cells were treated with a mock transfection, MIX30, or AG30 and analyzed for the induction of apoptosis. Following 24 h administration

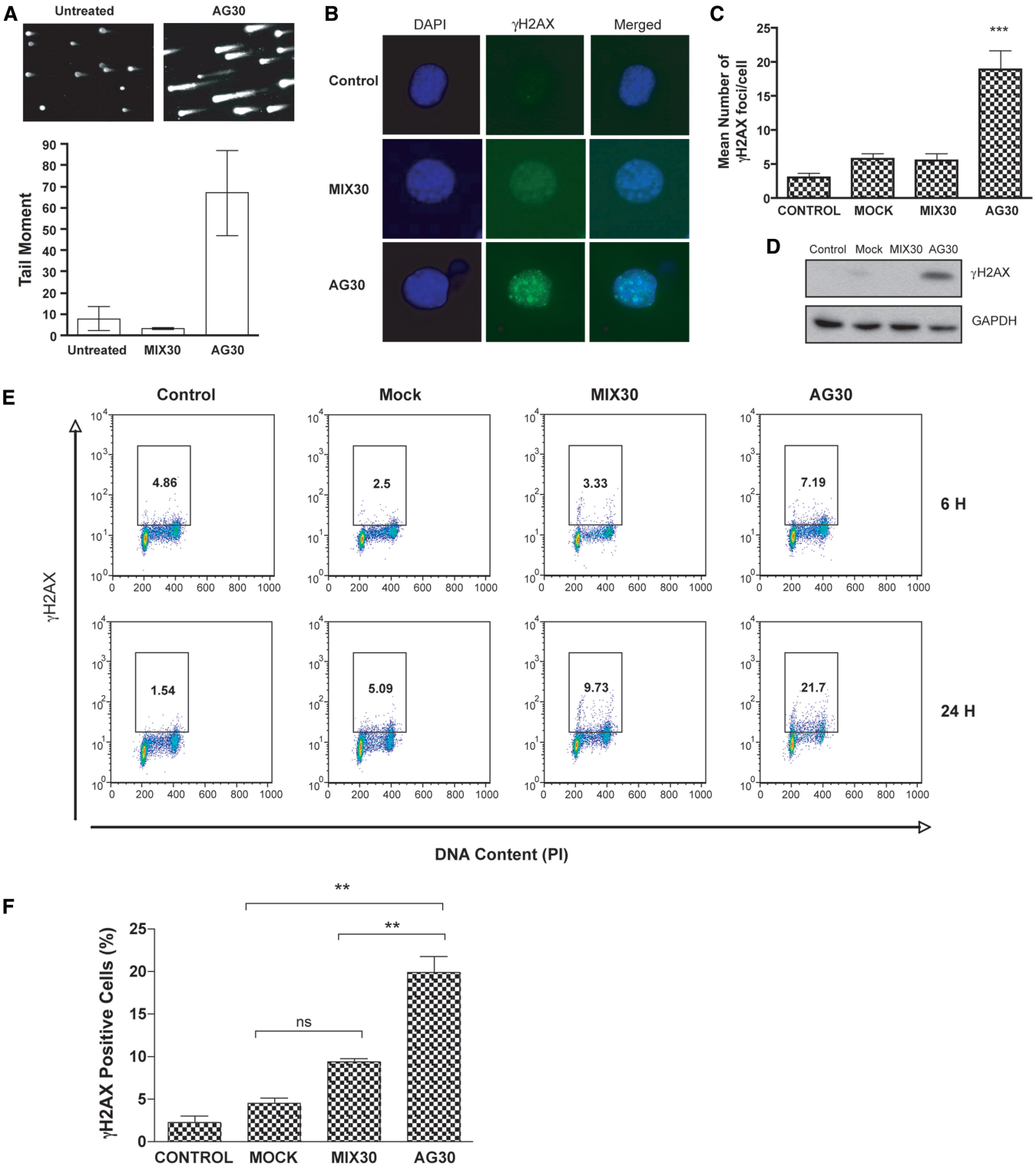

Figure 3. Triplex formation induces DSBs. (**A**) Neutral single cell comet assay of untreated and AG30-treated AV16 cells and measurement of comet tail moment 24 h posttreatment. 100–150 cells were evaluated per treatment (mean ± SEM). (**B**) Immunofluorescence of triplex-induced γH2AX foci 24 h posttreatment with MIX30 or AG30. (**C**) Quantification of γH2AX immunofluorescence. ***$P < 0.001$. (**D**) Western blot analysis of γH2AX protein levels 24 h post TFO treatment. (**E**) Flow cytometry profiles of AV16 cells stained for expression of γH2AX and propidium iodide (PI) to measure DNA content and identify phases of the cell cycle. Cells were harvested 6 h and 24 h after treatment. The box indicates the gate for high levels of γH2AX and numbers represent percentage of cells with high levels of γH2AX. (**F**) Increase in the percentage of γH2AX-positive cells 24 h following treatment with AG30. Data represent three independent experiments. **$P < 0.01$, ns = not significant.

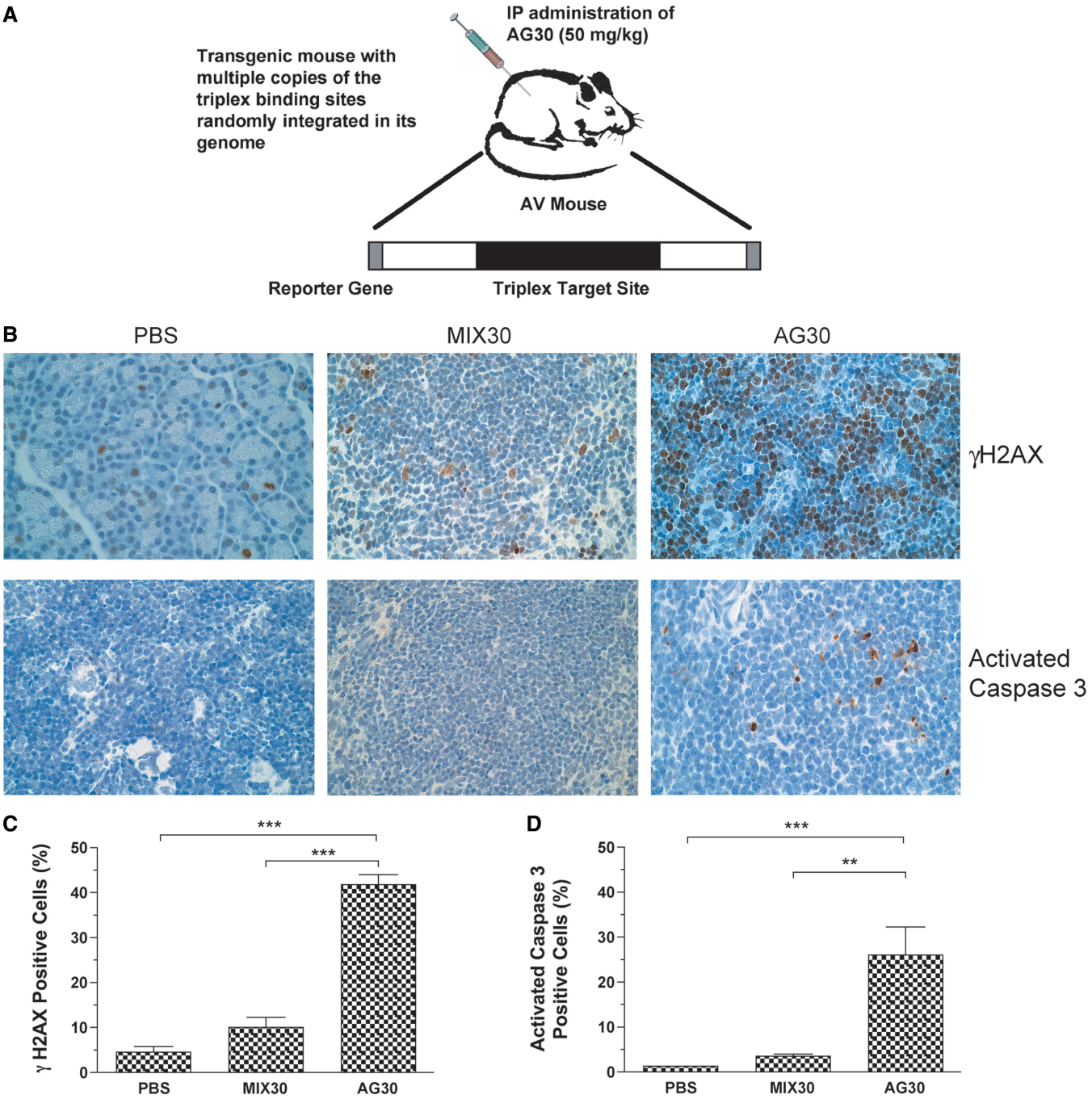

Figure 4. Triplex formation induced DSBs in transgenic mouse model. (**A**) Schematic of transgenic mouse model, AV, which contains ~50 copies of the triplex target site chromosomally integrated into its genome. (**B**) Immunohistochemistry of spleen samples harvested from AV mice 6 h posttreatment with MIX30 or AG30 (50 mg/kg). (**C, D**) Quantitation of immunohistochemical findings. $^{***}P < 0.001$, $^{**}P < 0.01$.

of AG30, 55% of the deficient cells were determined to be Annexin V positive compared with 32% of the AG30-treated NER-proficient cells (Figure 5B). Western blot analysis of cleaved PARP also indicated an increase in apoptotic cell death in the absence of XPA (Figure 5C). These findings suggest that XPA is not required for activation of apoptosis, despite its importance in the repair of triplex structures. Furthermore, we can conclude that a loss of XPA, and possibly functional NER, leads to an increase in apoptosis in response to triplex-induced DSBs.

XPD requirement for triplex-induced apoptosis

After determining that activation of apoptosis was a cellular response to extensive triplex-induced DNA strand breaks both *in vitro* and *in vivo*, we were interested in determining which proteins were involved in maintaining the switch from DNA repair to apoptosis. We hypothesized that a dual role NER protein like XPD, which contributes to genomic stability by participating in both repair and apoptosis, may also aid in triggering the cell to activate a pro-apoptotic pathway in the

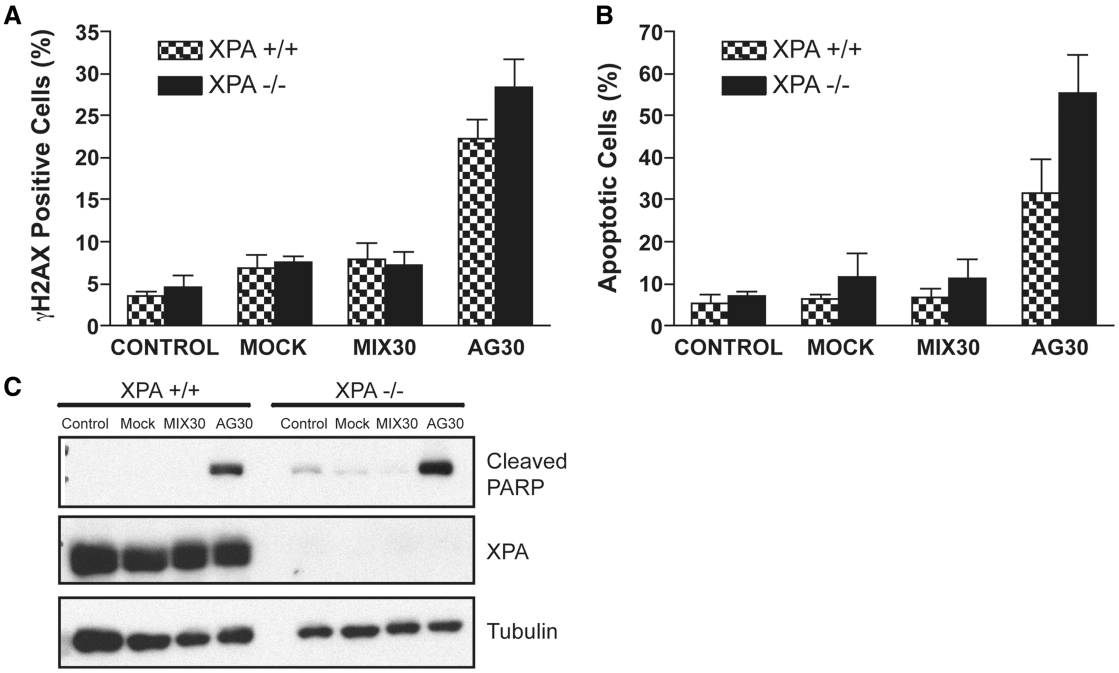

Figure 5. Role of XPA in the activation of triplex-induced apoptosis. (**A**) Analysis of γH2AX expression levels as a measure of triplex-induced DSBs in XPA-proficient and XPA-deficient cells 24 h post AG30 treatment. (**B**) Detection of Annexin V binding indicates an increase in apoptotic cell death in the absence of XPA 24 h posttreatment with 2 μg of oligonucleotides. (**C**) Western blot analysis of caspase-mediated cleavage of PARP as a measure of triplex-induced apoptosis.

presence of excessive triplex-induced DNA DSBs. AV16 cells proficient or deficient for XPD were treated with AG30 and analyzed for the activation of apoptosis. As expected, monolayer growth assays demonstrated a decrease in cell survival in the XPD-proficient cells (Figure 6A). However, a decrease in cell growth was not observed following TFO treatment of the siRNA XPD-depleted cells, where the level of cell growth was similar to that of control cells. To further attribute a role for XPD in activating apoptosis in response to excessive DNA strand breaks induced by triplex structures, we also evaluated the level of Annexin V-positive cells. AG30 treatment of siRNA XPD-depleted cells resulted in a significant decrease in apoptosis ($P < 0.001$) (Figure 6B). Western blot analysis of cleaved PARP also supports a reduction in triplex-induced apoptosis that is contingent on XPD (Figure 6C). To establish that the change in apoptosis did not result from siRNA off-target effects, we also evaluated cleaved PARP levels following AG30 treatment in AV16 cells that had been transfected with control siRNAs. This analysis revealed no reduction in the triplex-induced apoptosis levels in cells that had been treated with either nontarget or GAPDH siRNA controls compared with XPD-proficient cells (Supplementary Figure S3).

XPD helicase mediates strand separation at the site of the DNA lesion (34). In addition, tumor suppressor p53, a central component of apoptosis, can bind to and inhibit its helicase activity. After AG30 treatment, we determined by Western blot that an increase in p53 protein levels corresponded to increased caspase 3-mediated cleavage of PARP in XPD-proficient cells (Figure 6D). On the contrary, the relative amount of p53 protein remained stable following TFO treatment of XPD-depleted cells compared with untreated cells. Upon DNA damage, phosphorylation of p53 at serine 15 coordinates polyphosphorylation, maintains nuclear retention and stabilizes the protein through disruption of MDM2 binding (35–37). As determined by Western blot analysis, triplex-induced DNA strand breaks resulted in increased phosphorylation of serine 15 in XPD-proficient cells. However, a reduction in p53 phosphorylation at serine 15 was observed in the XPD-depleted cells (Figure 6E).

To investigate whether the differential induction of apoptosis in XPD-proficient and -deficient cells was the hallmark of a differential induction of DNA damage, we performed neutral comet assays. As shown, in Figure 6F, triplex formation induced the same degree of DSBs in XPD-proficient cells as it did in the XPD-depleted cells verifying that triplex-induced DNA strand breaks are not dependent on functional XPD. The results from these studies support a mechanism where XPD is important for activation of apoptosis and not required for the formation of triplex-induced DSBs.

Recruitment of XPD to the DSB site

XPD has been implicated in our studies to occupy an important role in activating apoptosis in response to triplex-induced DSBs. To determine whether XPD protein interacts with γH2AX foci, we treated AV16 cells with MIX30 or AG30. Confocal microscopy analysis indicates co-localization of XPD with γH2AX foci following treatment with the TFO, AG30 (Figure 7A). Calculation of a co-localization coefficient using ImageJ demonstrates that

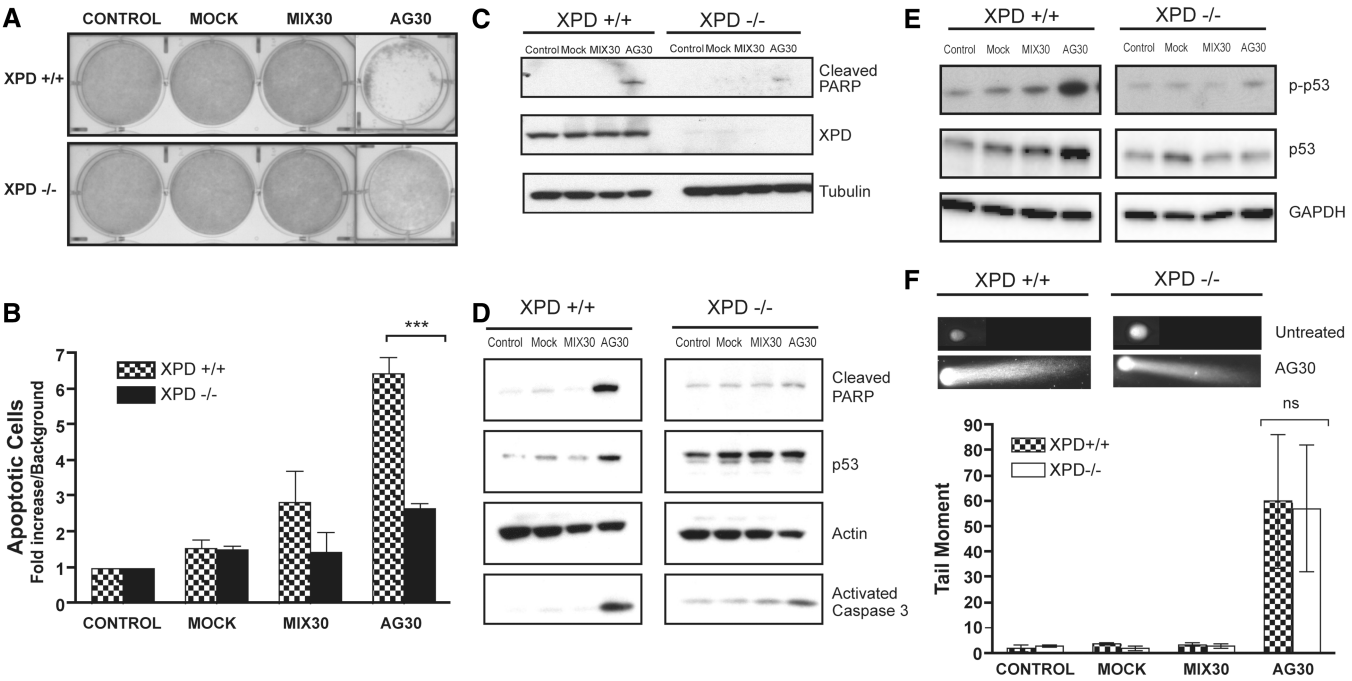

Figure 6. XPD is required for triplex-induced apoptosis. (**A**) Monolayer growth studies demonstrate that XPD-deficient cells are resistant to triplex-induced decrease in cell growth. (**B**) Knockdown of XPD results in significant reduction of induced apoptosis as measured by Annexin V staining (***$P < 0.001$). (**C**) Western blot analysis of activation of apoptosis as measured by cleaved PARP following siRNA knockdown of XPD. (**D**) Western blot analysis of triplex-induced apoptosis and effect on p53 levels. (**E**) Phosphorylation of p53 at serine 15 is reduced in XPD-knockdown cells in the presence of multiple triplex structures. (**F**) Neutral single cell comet assay of untreated and AG30-treated XPD-proficient and -deficient cells. Measurement of comet tail moment 24 h after treatment reveals similar levels of DSBs. 100-150 cells were evaluated per treatment (mean ± SEM), ns = not significant.

XPD is mobilized to the triplex-induced DSB site (Figure 7B). To further confirm XPD interactions with γH2AX foci, we treated AV16 cells with a mock transfection, MIX30 or AG30. Twenty-four hours after treatment, γH2AX was immunoprecipitated from cell lysates using proteinA/G beads and probed for XPD by Western blot analysis. In whole cell lysates, γH2AX was detected by Western blot analysis only in the AG30-treated cells and similar levels of XPD were observed in all of the treatment groups. However, Western blot analysis of the γH2AX-immunoprecipitation product revealed a signal for XPD in the AG30-treated AV16 cells that was substantially more robust than MIX30 treatment (Figure 7C). These findings suggest that XPD is recruited to the site of damage and further supports the confocal microscopy results (Figure 7C). The specificity of this interaction was confirmed with the absence of XPD and γH2AX in IgG co-immunoprecipitations (Supplementary Figure S4A).

To verify that XPD depletion did not inhibit the formation of γH2AX foci, thus resulting in a reduction in triplex-induced apoptosis, we evaluated γH2AX foci formation in XPD-proficient and -deficient cells following TFO treatment using immunofluorescence (Figure 7D). A similar mean number of γH2AX foci/cell was observed following AG30 treatment in the XPD-depleted cells compared with the proficient cells (Figure 7E). This implies that although XPD co-localizes at the DSB site, it is not required for γH2AX foci formation and supports our earlier data that show that XPD is not required for triplex-induced DSBs.

Activation of apoptosis preserves genomic integrity

Apoptosis plays an important role in maintaining genomic integrity by providing a mechanism by which a cell can actively control its own death in response to a variety of DNA-damaging stimuli. Xia *et al.* (38) and Cook *et al.* (39) have independently discovered that the phosphorylation status of the tyrosine 142 residue (Y142) of H2AX is critical in determining the relative recruitment of either DNA repair or pro-apoptotic factors to the site of DSBs. Both groups demonstrate that unlike S139, Y142 is phosphorylated in normal undamaged cells. When repair is possible following DNA damage, Y142 is gradually dephosphorylated, allowing the γH2AX (S139 phosphorylation) modification and the recruitment of repair factors to occur. However, in cases where DNA damage is excessive Y142-phosphorylated H2AX persists in the presence of S139 phosphorylation. This doubly phosphorylated H2AX recruits pro-apoptotic factors like the JNK complex, an established inducer of apoptosis.

To establish a role for Y142 phosphorylation in regulation of the apoptotic response following triplex-induced DNA strand breaks, we probed both H2AX phosphorylation sites by Western blot analysis. NER-proficient and XPA-deficient cells were treated with AG30, and 24 h posttreatment, cell lysates were prepared. As we observed in our previous experiments (Figure 5C),

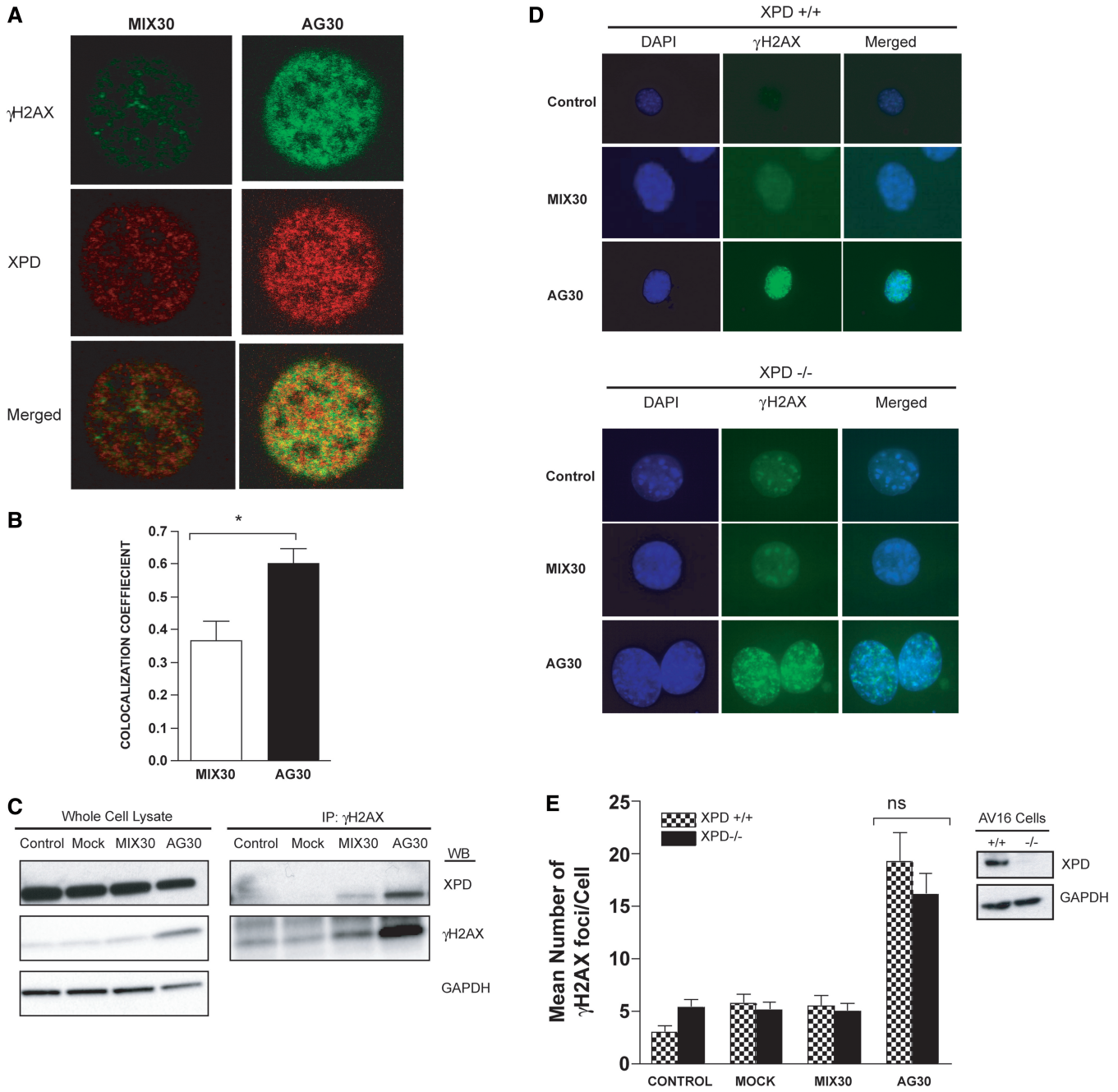

Figure 7. XPD is recruited to the γH2AX site. (**A**) Confocal microscopy indicates co-localization of XPD with γH2AX foci. (**B**) Co-localization coefficient calculated using NIH ImageJ software (*$P < 0.05$). (**C**) Co-immunoprecipitation of γH2AX with XPD by western blot analysis. (**D**) Immunofluorescence studies of γH2AX foci formation in XPD+/+ and XPD−/− cells 24 h post AG30 treatment. (**E**) Western blot analysis of XPD protein levels in proficient and deficient cells. Quantification of γH2AX foci formation per cell. Sixty to seventy cells were evaluated per treatment.

triplex-induced DNA strand breaks resulted in the activation of apoptosis in both cell lines as determined by the presence of cleaved PARP (Figure 8A). Although apoptosis was observed in both XPA-proficient and XPA-deficient cells following TFO treatment, slightly higher levels of S139 phosphorylation was observed in the XPA-deficient cells, suggesting the presence of more DSBs. In the case of the XPA-deficient cells, an increase in the level of Y142 phosphorylation is also observed, compared with the XPA-proficient cells (Figure 8A). Tyrosine 142 phosphorylation is a prerequisite for recruitment of the proteins necessary for apoptosis. These results correspond with our observation that there is a ~2-fold increase in apoptotic cells in XPA-deficient cells compared with XPA-proficient following AG30 treatment.

XPD-proficient and siRNA XPD-depleted cells were also treated with AG30, and 24 h posttreatment, cell lysates were prepared. As we observed in our previous

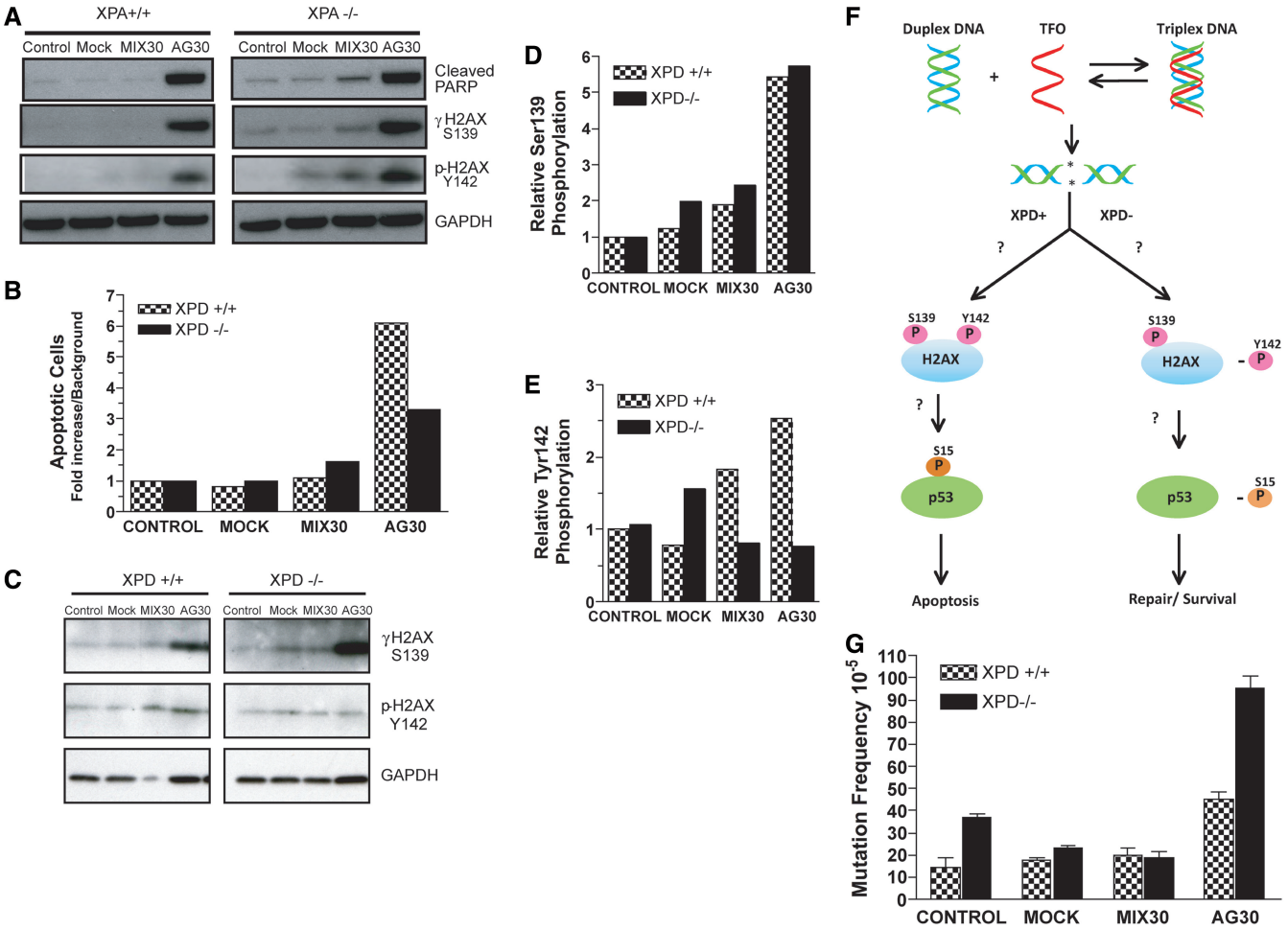

Figure 8. Activation of apoptosis minimizes triplex-induced genomic instability. (**A**) Western blot analysis of H2AX phosphorylation at serine 139 and tyrosine 142 in XPA-proficient and -deficient cells 24 h following AG30 treatment. (**B**) Analysis of triplex-induced apoptosis in XPD+/+ and XPD−/− cells as measured by Annexin V staining. (**C**) Western blot analysis of the phosphorylation status of H2AX at serine 139 and tyrosine 142 in XPD-proficient and -deficient cell 24 h following TFO treatment. (**D** and **E**) Quantification of the relative S139 and Y142 phosphorylation levels in XPD-deficient cells compared with XPD-proficient cells in response to triplex-induced DNA DSBs. (**F**) Schematic of XPD-dependent triplex-induced apoptosis. (**G**) Triplex-induced genomic instability as determined by mutation frequencies in the *supFG1* reporter gene in XPD +/+ and XPD −/− cells treated with TFOs. The frequency of mutations was calculated by dividing the number of colorless mutant plaques by the total number of plaques counted. Each experiment was performed in triplicate, and the standard errors were calculated for the mutation frequency. (mean ± SEM, $n = 3$).

experiments, when AV16 cells were XPD depleted using siRNA, there was a decrease in the level of apoptotic cells (Figure 8B). However, western blot analysis determined that the relative S139 phosphorylation level remained constant when XPD was depleted from the cells, although the induction of apoptosis was reduced (Figure 8C and D). This supports our hypothesis that the reduction in apoptosis levels observed in XPD-deficient cells can not be attributed to a decrease in triplex-induced DNA strand breaks and strongly supports that XPD is not required for triplex-induced DSBs. On the other hand, when the relative levels of Y142 phosphorylation were analyzed following TFO treatment there was a reduction in phosphorylation in the XPD-deficient cells, although the level of DNA DSBs was similar to that of the proficient cells (Figure 8C and E). These results correspond with our observation that there is a decrease in apoptotic cells in XPD-deficient cells compared with XPD-proficient following AG30 treatment. These data support a model in which H2AX phosphorylation at residues S139 and Y142 is required for activation of apoptosis in response to triplex-induced DSBs (Figure 8F). This would suggest that an absence of XPD disrupts the signaling pathway used to trigger apoptosis in the presence of DNA strand breaks induced by the formation of multiple triplex structures.

Following confirmation that apoptosis plays a key role in processing triplex-induced DNA DSBs, we proceeded to investigate its importance in preserving genomic integrity. Site-directed mutagenesis induced by triplex structures has been established *in vitro* and *in vivo* (40,41). Because cells defective in apoptosis tend to survive with excess damage, we examined the effect of XPD depletion on triplex-induced genomic instability. Using an assay for targeted mutagenesis in mammalian cells, we evaluated triplex-induced mutations using AV16 cells, which

contain ~100 copies of the λsupFG1 shuttle vector DNA in a chromosomal locus. Through the use of packaging extracts, the vector DNA can be isolated from genomic DNA into phage particles and subsequently analyzed for induced mutations. *SupFG1* not only encodes an amber suppressor tRNA whose function can be scored in indicator bacteria, but also contains the AG30 triplex-binding site (16).

AV16 and AV16 XPD-19-1 cells, which stably expressed XPD shRNA (Supplementary Figure S4B), were treated with a mock transfection, MIX30, or AG30 and analyzed for the induction of mutations 48 h posttreatment. We observed a mutation frequency (45×10^{-5}) in XPD-proficient cells following AG30 treatment that was ~2-fold higher than the frequency obtained from MIX30-treated XPD +/+ cells (20×10^{-5}) (Figure 8H). However, AG30 treatment (95×10^{-5}) of XPD-deficient cells resulted in a 5-fold increase in mutation frequency compared with XPD-deficient cells that received MIX30 treatment (19×10^{-5}) (Figure 8H). The increase in mutation frequency observed in the XPD-deficient cells may be attributed in part to the cells' inability to activate apoptosis. Taken together, these results position apoptosis as an important pathway in preserving genomic integrity in response to triplex-induced helical distortions.

DISCUSSION

Cells are faced with the fundamental decision of activating the appropriate ratio of DNA repair and apoptosis in response to damage. Our data suggest that the TFIIH protein, XPD, is involved in maintaining the balance between these two outcomes in response to the formation of altered helical structures. Thus, we provide evidence that the NER pathway is not only necessary for the repair of triplex structures, but is also important in the activation of pro-apoptotic pathways in response to helical distorting DNA structures. A key question exists as to how the cell determines when damage is excessive and how this determination triggers the shift from repair to apoptosis. The present study indicates that the absence of XPD results in a decrease in phosphorylation of the tyrosine 142 residue of H2AX in addition to p53. Recent work has determined that a balance between the kinase activity of WSTF and the phosphatase activity of Eya proteins help to regulate cellular fate following DNA damage (38,39). When repair is possible Y142 must be de-phosphorylated by Eya to allow for S139 phosphorylation and recruitment of repair proteins. Otherwise, Y142 phosphorylation persists causing the cell to activate apoptosis, thus eliminating the cells with irreversible damage.

Although studies indicate that Y142 is gradually dephosphorylated after DNA damage, it is possible that Y142 is re-phosphorylated after futile attempts to repair the excessive DNA damage to facilitate apoptosis. It is theoretically possible that if XPD is not present to trigger the switch to activate apoptosis, this re-phosphorylation does not take place and the remaining DNA damage response proteins necessary for apoptosis are not recruited. Chymkowitch *et al.* (42) have recently shown that the TFIIH complex is able to phosphorylate the androgen receptor at position AR/S515 via cdk7. Additionally, mutations in the C-terminal domain of XPD were found to disturb the architecture of TFIIH leading to the dysregulation of cdk7-related phosphorylation (43,44). Taken together, these findings along with our result that XPD co-localizes with γH2AX provide support for an XPD-dependent apoptotic pathway.

The XPD protein has been identified as having a role in NER, transcription and possibly cell cycle. However, XPD also exists in non-TFIIH complexes, such as CAK–XPD and MMXD and has function in other cellular processes, including apoptosis. Knockdown of XPD did not reduce the intensity of triplex-induced DSBs or γH2AX foci formation, although a significant decrease in apoptosis was observed. It is apparent from the work presented that key proteins, which contribute to cellular survival through their involvement in DNA repair, also participate in the mechanism that shifts the cell from DNA repair to apoptosis.

Intramolecular triplex DNA structures exist transiently in genomic DNA and represent an endogenous source of genomic instability. Naturally occurring sequences capable of forming H-DNA are typically located in promoters and exons and are believed to be involved in the regulation of expression of several disease-linked genes (45–48). The human *c-myc* gene, which is often translocated and overexpressed in tumors, contains an H-DNA forming sequence in its promoter (45). Many breakpoints on the translocated *c-myc* gene are clustered around the H-DNA forming sequence in the promoter region in Burkitt's lymphoma (14). Studies suggest that noncanonical structures result in fragile sites or mutation hotspots, and can lead to DSBs and subsequent translocation of the gene. The maintenance of a mechanism by which the cell can actively determine cellular fate in response to the formation of these structures may be of central importance for avoiding progression to cancer, because the default mechanism of apoptosis prevents expansion of cells in which unrepaired damage would lead to mutation and to carcinogenesis. Additionally, we can also hypothesize that XPD may be an integral component in determining the fate of cells assaulted by other NER-recognized DNA damage including those induced by UV. This study highlights the complexity of the balance between DNA repair and apoptosis in response to damage induced by altered helical structures.

SUPPLEMENTARY DATA

Supplementary Data are available at NAR Online.

ACKNOWLEDGEMENTS

We are grateful to P. Glazer, J. Sweasy, D. Kidane, M. Menezes, and J. Lloyd for helpful suggestions. We also thank P. Glazer for XPA +/+ and XPA −/− cells and for the XPA antibody.

FUNDING

National Institutes of Health [K22 CA120049, K22 CA120049-03S1 to F.A.R.]; American Cancer Society [IRG 58-012-51 to F.A.R.]; Kingsley Fellowship in Medical Research (to F.A.R.). Funding for open access charge: Institutional funds.

Conflict of interest statement. None declared.

REFERENCES

1. Bernstein,C., Bernstein,H., Payne,C.M. and Garewal,H. (2002) DNA repair/pro-apoptotic dual-role proteins in five major DNA repair pathways: fail-safe protection against carcinogenesis. *Mutat. Res.*, **511**, 145–178.
2. de Laat,W.L., Jaspers,N.G. and Hoeijmakers,J.H. (1999) Molecular mechanism of nucleotide excision repair. *Genes Dev.*, **13**, 768–785.
3. Wang,X.W., Vermeulen,W., Coursen,J.D., Gibson,M., Lupold,S.E., Forrester,K., Xu,G., Elmore,L., Yeh,H., Hoeijmakers,J.H. *et al*. (1996) The XPB and XPD DNA helicases are components of the p53-mediated apoptosis pathway. *Genes Dev.*, **10**, 1219–1232.
4. Robles,A.I., Wang,X.W. and Harris,C.C. (1999) Drug-induced apoptosis is delayed and reduced in XPD lymphoblastoid cell lines: possible role of TFIIH in p53-mediated apoptotic cell death. *Oncogene*, **18**, 4681–4688.
5. Wang,X.W., Yeh,H., Schaeffer,L., Roy,R., Moncollin,V., Egly,J.M., Wang,Z., Freidberg,E.C., Evans,M.K., Taffe,B.G. *et al*. (1995) p53 modulation of TFIIH-associated nucleotide excision repair activity. *Nat. Genet.*, **10**, 188–195.
6. Wang,G., Seidman,M.M. and Glazer,P.M. (1996) Mutagenesis in mammalian cells induced by triple helix formation and transcription-coupled repair. *Science*, **271**, 802–805.
7. Rogers,F.A., Vasquez,K.M., Egholm,M. and Glazer,P.M. (2002) Site-directed recombination via bifunctional PNA-DNA conjugates. *Proc. Natl. Acad. Sci. USA*, **99**, 16695–16700.
8. Watson,J.D. and Crick,F.H. (1974) Molecular structure of nucleic acids: a structure for deoxyribose nucleic acid. J.D. Watson and F.H.C. Crick. Published in Nature, number 4356 April 25, 1953. *Nature*, **248**, 765.
9. Htun,H. and Dahlberg,J.E. (1988) Single strands, triple strands, and kinks in H-DNA. *Science*, **241**, 1791–1796.
10. Voloshin,O.N., Mirkin,S.M., Lyamichev,V.I., Belotserkovskii,B.P. and Frank-Kamenetskii,M.D. (1988) Chemical probing of homopurine-homopyrimidine mirror repeats in supercoiled DNA. *Nature*, **333**, 475–476.
11. Mirkin,S.M., Lyamichev,V.I., Drushlyak,K.N., Dobrynin,V.N., Filippov,S.A. and Frank-Kamenetskii,M.D. (1987) DNA H form requires a homopurine-homopyrimidine mirror repeat. *Nature*, **330**, 495–497.
12. Schroth,G.P. and Ho,P.S. (1995) Occurrence of potential cruciform and H-DNA forming sequences in genomic DNA. *Nucleic Acids Res.*, **23**, 1977–1983.
13. Wang,G. and Vasquez,K.M. (2004) Naturally occurring H-DNA-forming sequences are mutagenic in mammalian cells. *Proc. Natl. Acad. Sci. USA*, **101**, 13448–13453.
14. Saglio,G., Grazia Borrello,M., Guerrasio,A., Sozzi,G., Serra,A., di Celle,P.F., Foa,R., Ferrarini,M., Roncella,S., Borgna Pignatti,C. *et al*. (1993) Preferential clustering of chromosomal breakpoints in Burkitt's lymphomas and L3 type acute lymphoblastic leukemias with a t(8;14) translocation. *Genes Chromosomes Cancer*, **8**, 1–7.
15. Knauert,M.P., Lloyd,J.A., Rogers,F.A., Datta,H.J., Bennett,M.L., Weeks,D.L. and Glazer,P.M. (2005) Distance and affinity dependence of triplex-induced recombination. *Biochemistry*, **44**, 3856–3864.
16. Rogers,F.A., Manoharan,M., Rabinovitch,P., Ward,D.C. and Glazer,P.M. (2004) Peptide conjugates for chromosomal gene targeting by triplex-forming oligonucleotides. *Nucleic Acids Res.*, **32**, 6595–6604.
17. Stachelek,G.C., Dalal,S., Donigan,K.A., Campisi Hegan,D., Sweasy,J.B. and Glazer,P.M. (2010) Potentiation of temozolomide cytotoxicity by inhibition of DNA polymerase beta is accentuated by BRCA2 mutation. *Cancer Res.*, **70**, 409–417.
18. Rogers,F.A., Lin,S.S., Hegan,D.C., Krause,D.S. and Glazer,P.M. (2012) Targeted gene modification of hematopoietic progenitor cells in mice following systemic administration of a PNA-peptide conjugate. *Mol. Ther.*, **20**, 109–118.
19. Gunther,E.J., Yeasky,T.M., Gasparro,F.P. and Glazer,P.M. (1995) Mutagenesis by 8-methoxypsoralen and 5-methylangelicin photoadducts in mouse fibroblasts: mutations at cross-linkable sites induced by offoadducts as well as cross-links. *Cancer Res.*, **55**, 1283–1288.
20. Wang,G., Chen,Z., Zhang,S., Wilson,G.L. and Jing,K. (2001) Detection and determination of oligonucleotide triplex formation-mediated transcription-coupled DNA repair in HeLa nuclear extracts. *Nucleic Acids Res.*, **29**, 1801–1807.
21. Macris,M.A. and Glazer,P.M. (2003) Transcription dependence of chromosomal gene targeting by triplex-forming oligonucleotides. *J. Biol. Chem.*, **278**, 3357–3362.
22. Johnson,M.D. III and Fresco,J.R. (1999) Third-strand in situ hybridization (TISH) to non-denatured metaphase spreads and interphase nuclei. *Chromosoma*, **108**, 181–189.
23. Schwartz,T.R., Vasta,C.A., Bauer,T.L., Parekh-Olmedo,H. and Kmiec,E.B. (2008) G-rich oligonucleotides alter cell cycle progression and induce apoptosis specifically in OE19 esophageal tumor cells. *Oligonucleotides*, **18**, 51–63.
24. Qi,H., Lin,C.P., Fu,X., Wood,L.M., Liu,A.A., Tsai,Y.C., Chen,Y., Barbieri,C.M., Pilch,D.S. and Liu,L.F. (2006) G-quadruplexes induce apoptosis in tumor cells. *Cancer Res.*, **66**, 11808–11816.
25. Do,N.Q., Lim,K.W., Teo,M.H., Heddi,B. and Phan,A.T. (2011) Stacking of G-quadruplexes: NMR structure of a G-rich oligonucleotide with potential anti-HIV and anticancer activity. *Nucleic Acids Res.*, **39**, 9448–9457.
26. Kutyavin,I.V., Lokhov,S.G., Afonina,I.A., Dempcy,R., Gall,A.A., Gorn,V.V., Lukhtanov,E., Metcalf,M., Mills,A., Reed,M.W. *et al*. (2002) Reduced aggregation and improved specificity of G-rich oligodeoxyribonucleotides containing pyrazolo[3,4-d]pyrimidine guanine bases. *Nucleic Acids Res.*, **30**, 4952–4959.
27. Shah,G.M., Shah,R.G. and Poirier,G.G. (1996) Different cleavage pattern for poly(ADP-ribose) polymerase during necrosis and apoptosis in HL-60 cells. *Biochem. Biophys. Res. Commun.*, **229**, 838–844.
28. Rogakou,E.P., Pilch,D.R., Orr,A.H., Ivanova,V.S. and Bonner,W.M. (1998) DNA double-stranded breaks induce histone H2AX phosphorylation on serine 139. *J. Biol. Chem.*, **273**, 5858–5868.
29. Fernandez-Capetillo,O., Lee,A., Nussenzweig,M. and Nussenzweig,A. (2004) H2AX: the histone guardian of the genome. *DNA Repair*, **3**, 959–967.
30. Huang,X., Okafuji,M., Traganos,F., Luther,E., Holden,E. and Darzynkiewicz,Z. (2004) Assessment of histone H2AX phosphorylation induced by DNA topoisomerase I and II inhibitors topotecan and mitoxantrone and by the DNA cross-linking agent cisplatin. *Cytometry A*, **58**, 99–110.
31. Cleaver,J.E. (2011) gammaH2Ax: biomarker of damage or functional participant in DNA repair "all that glitters is not gold!". *Photochem. Photobiol.*, **87**, 1230–1239.
32. Huang,X., Halicka,H.D., Traganos,F., Tanaka,T., Kurose,A. and Darzynkiewicz,Z. (2005) Cytometric assessment of DNA damage in relation to cell cycle phase and apoptosis. *Cell Prolif.*, **38**, 223–243.
33. Batty,D.P. and Wood,R.D. (2000) Damage recognition in nucleotide excision repair of DNA. *Gene*, **241**, 193–204.
34. de Boer,J., Donker,I., de Wit,J., Hoeijmakers,J.H. and Weeda,G. (1998) Disruption of the mouse xeroderma pigmentosum group D DNA repair/basal transcription gene results in preimplantation lethality. *Cancer Res.*, **58**, 89–94.
35. Kapoor,M., Hamm,R., Yan,W., Taya,Y. and Lozano,G. (2000) Cooperative phosphorylation at multiple sites is required to activate p53 in response to UV radiation. *Oncogene*, **19**, 358–364.

36. Shieh,S.Y., Ikeda,M., Taya,Y. and Prives,C. (1997) DNA damage-induced phosphorylation of p53 alleviates inhibition by MDM2. *Cell*, **91**, 325–334.
37. Steegenga,W.T., van der Eb,A.J. and Jochemsen,A.G. (1996) How phosphorylation regulates the activity of p53. *J. Mol. Biol.*, **263**, 103–113.
38. Xiao,A., Li,H., Shechter,D., Ahn,S.H., Fabrizio,L.A., Erdjument-Bromage,H., Ishibe-Murakami,S., Wang,B., Tempst,P., Hofmann,K. *et al.* (2009) WSTF regulates the H2A.X DNA damage response via a novel tyrosine kinase activity. *Nature*, **457**, 57–62.
39. Cook,P.J., Ju,B.G., Telese,F., Wang,X., Glass,C.K. and Rosenfeld,M.G. (2009) Tyrosine dephosphorylation of H2AX modulates apoptosis and survival decisions. *Nature*, **458**, 591–596.
40. Vasquez,K.M., Narayanan,L. and Glazer,P.M. (2000) Specific mutations induced by triplex-forming oligonucleotides in mice. *Science*, **290**, 530–533.
41. Vasquez,K.M., Wang,G., Havre,P.A. and Glazer,P.M. (1999) Chromosomal mutations induced by triplex-forming oligonucleotides in mammalian cells. *Nucleic Acids Res.*, **27**, 1176–1181.
42. Chymkowitch,P., Le May,N., Charneau,P., Compe,E. and Egly,J.M. The phosphorylation of the androgen receptor by TFIIH directs the ubiquitin/proteasome process. *EMBO J.*, **30**, 468–479.
43. Keriel,A., Stary,A., Sarasin,A., Rochette-Egly,C. and Egly,J.M. (2002) XPD mutations prevent TFIIH-dependent transactivation by nuclear receptors and phosphorylation of RARalpha. *Cell*, **109**, 125–135.
44. Compe,E., Drane,P., Laurent,C., Diderich,K., Braun,C., Hoeijmakers,J.H. and Egly,J.M. (2005) Dysregulation of the peroxisome proliferator-activated receptor target genes by XPD mutations. *Mol. Cell. Biol.*, **25**, 6065–6076.
45. Kinniburgh,A.J. (1989) A cis-acting transcription element of the c-myc gene can assume an H-DNA conformation. *Nucleic Acids Res.*, **17**, 7771–7778.
46. Pestov,D.G., Dayn,A., Siyanova,E., George,D.L. and Mirkin,S.M. (1991) H-DNA and Z-DNA in the mouse c-Ki-ras promoter. *Nucleic Acids Res.*, **19**, 6527–6532.
47. Bacolla,A., Jaworski,A., Connors,T.D. and Wells,R.D. (2001) Pkd1 unusual DNA conformations are recognized by nucleotide excision repair. *J. Biol. Chem.*, **276**, 18597–18604.
48. Belotserkovskii,B.P., De Silva,E., Tornaletti,S., Wang,G., Vasquez,K.M. and Hanawalt,P.C. (2007) A triplex-forming sequence from the human c-MYC promoter interferes with DNA transcription. *J. Biol. Chem.*, **282**, 32433–32441.